Supplementary Information †

Performance enhancement of supercapacitor negative electrode based on loofah sponge derived oxygen rich carbon through encapsulation of MoO_3 nanoflowers

Akanksha Joshi, Vikrant Sahu, Gurmeet Singh* and Raj Kishore Sharma**

Department of Chemistry, University of Delhi, Delhi-110007, INDIA

The equations used to evaluate supercapacitor cell performance through Charge-Discharge measurements.[1]

$$C_{sp} = \int_{E1}^{E2} i(E)\, dE / 2(E2 - E1)m\vartheta \quad \textbf{(1)}$$

$$C_m = \frac{I \times \Delta t}{m \times \Delta V} \quad \textbf{(2)}$$

$$E = \frac{0.5 \times C_m (\Delta V)^2}{3.6} \quad \textbf{(3)}$$

$$P = \frac{E \times 3600}{\Delta t} \quad \textbf{(4)}$$

where, C_{sp} is the specific capacitance (F g^{-1}), $\int_{E1}^{E2} i(E)\, dE$ is the integration of positive and negative sweep**,** *i(E)* is the instantaneous current, E1 and E2 are the cutoff potential of cyclic voltammetry, E2 − E1 is the working potential range, ϑ is the scan rate, C_m capacitance of cell in F g^{-1}, I is the current in m A, Δt is discharge time in s, m is active mass on two electrode in mg, ΔV is the voltage after IR drop in V, E is the energy density in Wh Kg^{-1}, and P is the power density in W Kg^{-1}.

To determine the mechanism behind charge storage Power's law is implied using equation:[2]

$$i\,(V) = a\vartheta^{b} \qquad \textbf{(5)}$$

Here, ***a*** and ***b*** are adjustable parameters and ***υ*** is the scan rate (V s^{-1}).

The following equation determines the contribution of current from capacitive and intercalation mechanism.[3]

$$i\,(V) = k_1(\vartheta) + k_2\,(\vartheta)^{\frac{1}{2}} \qquad \textbf{(6)}$$

The value of $k_1(\upsilon)$ and $k_2(\upsilon)^{1/2}$ gives the current contribution from capacitive and diffusion controlled intercalation mechanism respectively.

The maximum specific capacitance was calculated from the low frequency data of Nyquist plot using equation:[4]

$$C_{dm} = \frac{-1}{2\pi f Z'' m} \qquad \textbf{(7)}$$

Here, $\boldsymbol{C_{dm}}$ is specific capacitance**,** $\boldsymbol{Z''}$ imaginary part of the impedance, ***f*** is subsequent frequency, ***m*** mass of the electrode material.

This $\boldsymbol{C_{dm}}$ is further used to determine electrochemically active surface (ESA) area by equation:[5]

$$S_E = \frac{C_{dm}}{C_d} \qquad \textbf{(8)}$$

where, C_{dm} is obtained from the impedance data and C_d is a constant value of 20 μF cm^{-2}.

Randles plot determines the diffusion coefficient of electrode material using following equations:[6]

$$Z' = R_s + R_{ct} + \sigma_w . \omega^{-0.5} \qquad \textbf{(9)}$$

$$D_w = \left[\frac{RT}{\sqrt{2}AF^2\sigma_w C}\right]^2 \qquad \textbf{(10)}$$

Here, ω is angular frequency, σ_w corresponds to Warburg impedance coefficient and R_{ct} and R_s are charge transfer resistance and solution resistance respectively. D_w denotes diffusion coefficient in $cm^2\ s^{-1}$, R gas constant in $J\ K^{-1}\ mol^{-1}$, A area of electrode in cm^2, T absolute temperature in K, F Faraday constant in $C\ mol^{-1}$.

The conductivity of AC and 20 AC-MO is determined using the following equations:

$$R = \rho \frac{l}{a} \quad (11)$$

From the I-V plot, resistance (R) is determined and then from the above equation is used to find the resistivity (ρ). Conductivity is inverse of the resistivity (ρ).

Sample	N (%)	C (%)	H (%)	S (%)	O (%)
AC	0.00	50.69	4.034	0.257	45.01

Table S1. CHNS analysis of Activated carbon (AC).

Element	Position BE (eV)	FWHM (eV)	Raw area (cps eV)	RSF	Atomic mass	Atomic conc (%)	Mass conc (%)
C 1s	284.60	3.403	26453.3	0.278	12.011	86.28	82.52
O 1s	532.60	4.461	12906.7	0.780	15.999	13.72	17.48

Table S2. Quantification report of Activated carbon (AC).

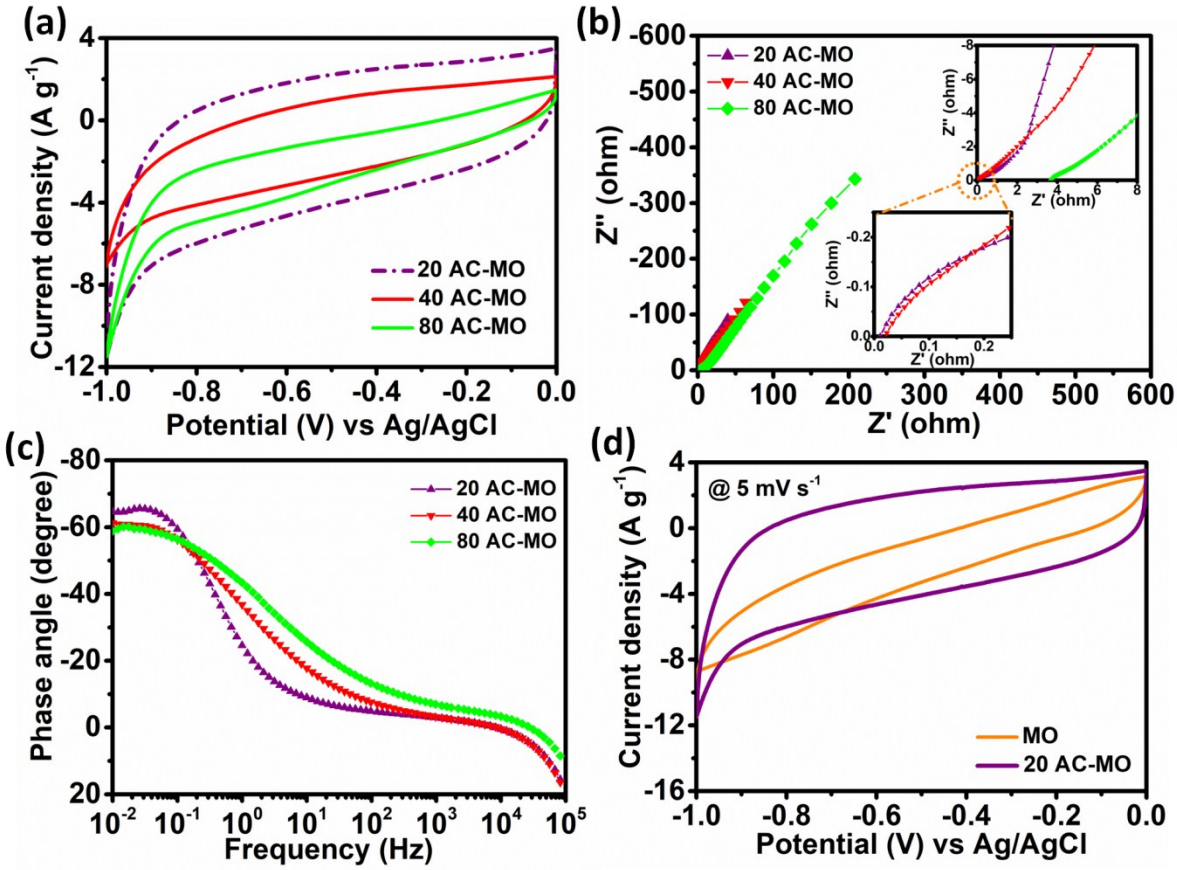

Fig S1. (a) Comparative voltammograms @ 5 mV s^{-1}. (b) Nyquist plot. (c) Bode plot. (d) Comparison of MO and 20 AC-MO voltammograms.

The electrochemical performance of different AC:MO samples is investigated and the voltammograms are presented in Figure S1. Out of three composites electrodes, 20 AC-MO show larger current response. The oxygen functional groups in AC matrix and open nanoflower configuration offer additional active sites and optimum charge storage in 20 AC-MO composite indicating the balanced in ionic as well as electronic conductivity. Figure S1b, the Nyquist plot shows the minimum resistance (inset Figure S1c) in case of 20 AC-MO, which is based on the calculated values of R_1 (solution resistance), R_2 (charge transfer resistance), C_1 (double layer capacitance) and W_1(warburg resistance) from the displayed equivalent circuit and is given in the table:

Sample	R_1 (ohm)	R_2 (ohm)	C_1 (Farad)	W_1 (ohm)
20 AC-MO	3.07	0.35	0.0005	7.82
40 AC-MO	2.60	0.35	0.0004	20
80 AC-MO	3.67	0.5	0.0003	25

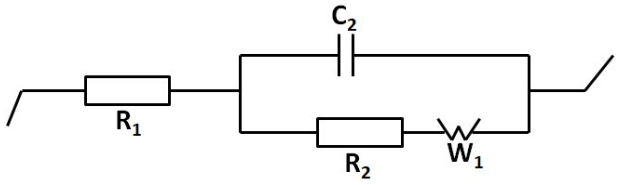

Likewise, bode plot in Figure S1c, illustrate more capacitive nature of 20 AC-MO with the highest bode angle (-65°). Despite of better conductivity of activated carbon (AC), the increase in content of carbon results in increase of overall resistance due to the uneven distribution of MoO3 nanostructures. As MoO3 nanostructure also reduces the diffusion distance of ions and hence results in a better performance of 20 AC-MO. Consequently, 20 AC-MO shows enhanced current as compared to the bare MoO_3 (MO) in voltammograms (Figure S1d).

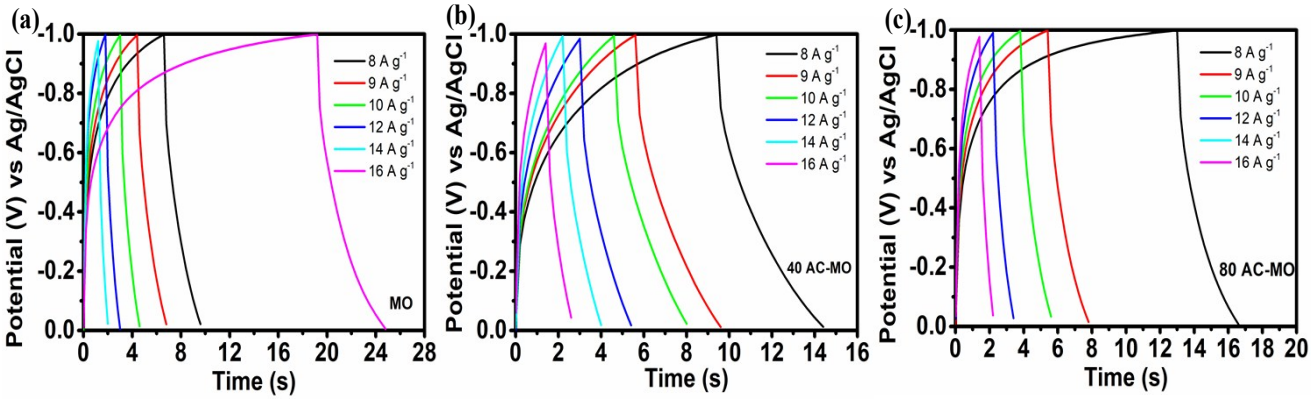

Fig. S2 Charge discharge measurement of (a) MO (b) 40 AC-MO (c) 80 AC-MO.

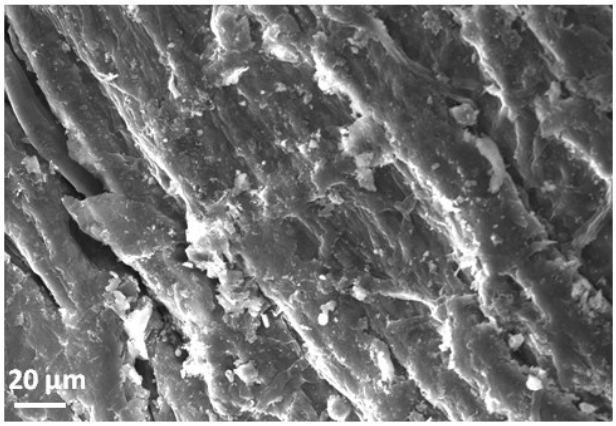

Fig. S3 SEM image of loofah sponge.

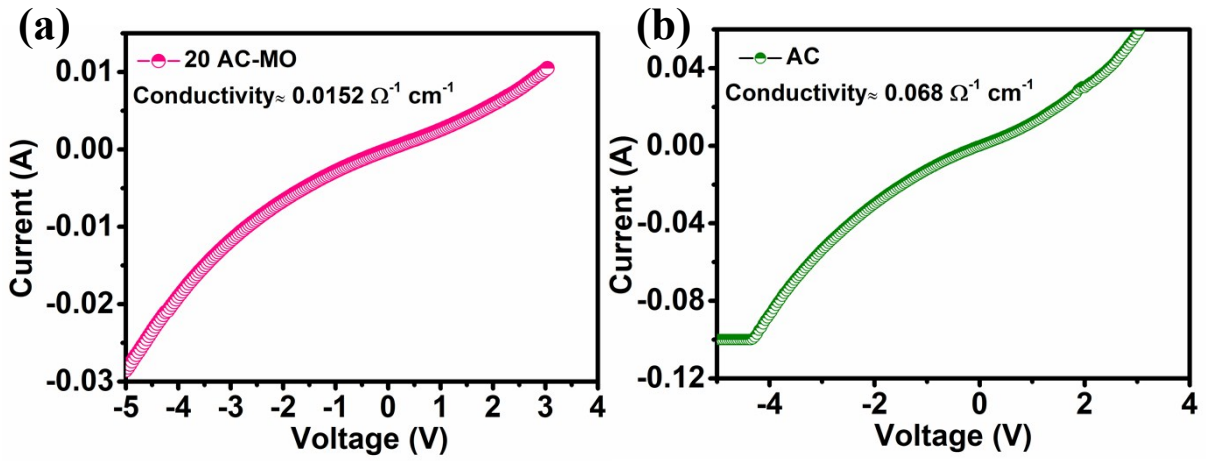

Fig. S4 I-V measurement of (a) 20 AC-MO (b) AC.

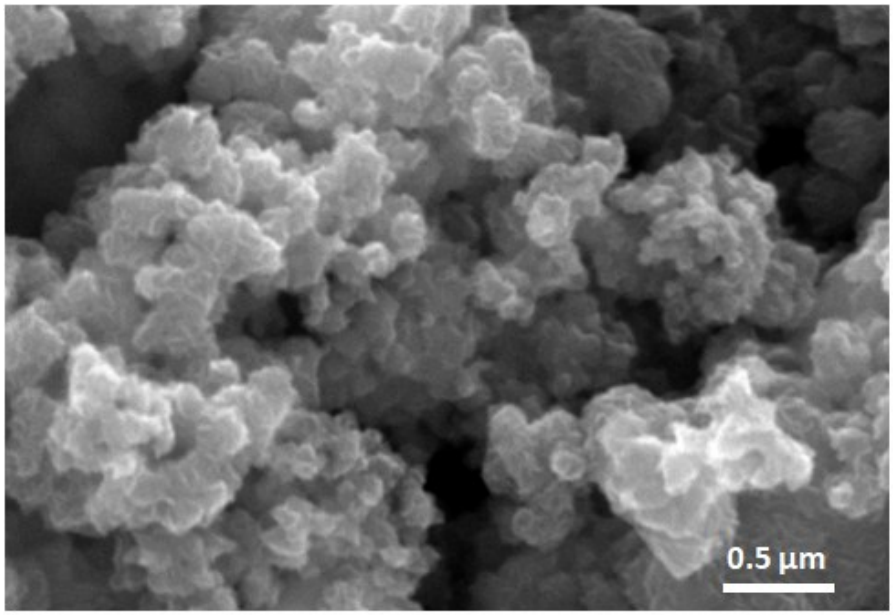

Fig. S5 SEM image of MoO3 (MO).

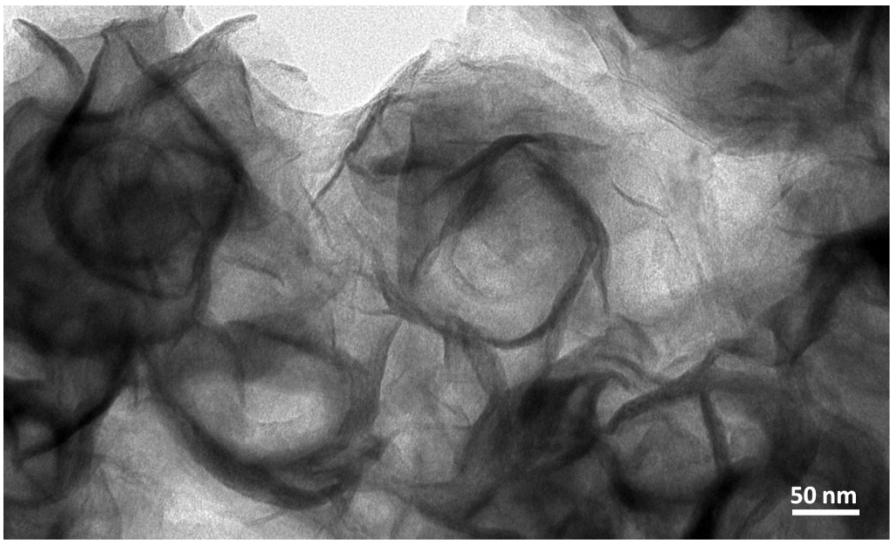

Fig. S6 TEM image of 20 AC-MO.

Formation mechanism of MoO_3 (MO) onto the activated carbon (AC)

When the $(NH_4)_6(Mo)_7O_{24}$, which acts as Mo^{6+} ion source, was dissolved into the activated carbon dispersion, it produces MoO_4^{2-} after certain time during hydrothermal process and in the mean time thiourea also produces S^{2-} and reacts with above solution to form MoS_3 which then decomposed to form MoO_3. In this process, first the MoO_3 nuclei is generated, which subsequently grows to nanosheets. As the hydrothermal time prolonged, the thin nanosheets self-assembled gradually and form stacking flower-like spherical MoO_3 structures onto the activated carbon scaffold.[7]

References

[1] V. Sahu, M. Mishra, G. Singh, R. K. Sharma, Turning Hazardous Diesel Soot into High Performance Carbon/MnO_2 Supercapacitive Energy Storage Material, ACS Sustainable Chem. Eng. 5 (2017) 450−459.

[2] K. V. Sankar, S. Surendran, K. Pandi, A. M. Allin, V. D. Nithya, Y. S. Lee, Selvan,

R. K. Studies on the electrochemical intercalation/de-intercalation mechanism of $NiMn_2O_4$ for high stable pseudocapacitor electrodes, RSC Adv. 5 (2015) 27649–27656.

[3] M. Sathiya, A. S. Prakash, K. Ramesh, J. M. Tarascon, A. K. Shukla, V_2O_5-Anchored Carbon Nanotubes for Enhanced Electrochemical Energy Storage, J. Am. Chem. Soc. 133 (2011)1629–16299.

[4] J. Zhang, X. S. Zhao, On the Configuration of Supercapacitors for Maximizing Electrochemical Performance, ChemSusChem 5 (2012) 818–841.

[5] W. Sugimoto, H. Iwata, Y. Yasunaga, Y. Murakami, Y. Takasu, Preparation of Ruthenic Acid Nanosheets and Utilization of Its Interlayer Surface for Electrochemical Energy Storage, Angew. Chem. Int. Ed. 42 (2003) 4092–4096.

[6] S. Lalwani, V. Sahu, R. B. Marichi, G. Singh, R. K. Sharma, In situ immobilized, magnetite nanoplatelets over holey graphene nanoribbons for high performance solid state supercapacitor, Electrochimica Acta 224 (2017) 517–526.

[7] Y. Liu, W. Zheng, Facile synthesis of 3D flower-like MoO3 and its gas sensor application, J Mater Sci: Mater Electron 27 (2016) 12996–13001.